

8-15-2017

The uppermost mantle seismic velocity and viscosity structure of central West Antarctica

J. P. O'Donnell
University of Leeds

K. Selway
University of Oslo

A. A. Nyblade
Pennsylvania State University

R. A. Brazier
Pennsylvania State University

D. A. Wiens
Washington University in St. Louis

See next page for additional authors

Follow this and additional works at: <https://digitalcommons.cwu.edu/cotsfac>



Part of the [Geomorphology Commons](#), [Geophysics and Seismology Commons](#), [Glaciology Commons](#), and the [Tectonics and Structure Commons](#)

Recommended Citation

O'Donnell, J. P., Selway, K., Nyblade, A. A., Brazier, R. A., Wiens, D. A., Anandakrishnan, S., Aster, R. C., Huerta, A. D., Wilson, T., & Winberry, J. P. (2017). The uppermost mantle seismic velocity and viscosity structure of central West Antarctica. *Earth and Planetary Science Letters*, 472, 38–49. <https://doi.org/10.1016/j.epsl.2017.05.016>

This Article is brought to you for free and open access by the College of the Sciences at ScholarWorks@CWU. It has been accepted for inclusion in All Faculty Scholarship for the College of the Sciences by an authorized administrator of ScholarWorks@CWU. For more information, please contact scholarworks@cwu.edu.

Authors

J. P. O'Donnell, K. Selway, A. A. Nyblade, R. A. Brazier, D. A. Wiens, S. Anandakrishnan, R. C. Aster, Audrey D. Huerta, T. Wilson, and J. Paul Winberry

The uppermost mantle seismic velocity and viscosity structure of central West Antarctica

J. P. O'Donnell^{1,2}, K. Selway^{3,†}, A. A. Nyblade¹, R. A. Brazier¹, D. A. Wiens⁴, S. Anandakrishnan¹, R. C. Aster⁵, A. D. Huerta⁶, T. Wilson⁷
and J. P. Winberry⁶

(May 10, 2017)

(1) Department of Geosciences, The Pennsylvania State University, University Park, PA 16802, USA

(2) School of Earth and Environment, The University of Leeds, Leeds, LS2 9JT, UK

(3) The Centre for Earth Evolution and Dynamics, The University of Oslo, 0316 Oslo, Norway

(4) Department of Earth and Planetary Sciences, Washington University, St. Louis, MO 63160, USA

(5) Department of Geosciences, Colorado State University, Fort Collins, CO 80523, USA

(6) Department of Geological Sciences, Central Washington University, Ellensburg, WA 98926, USA

(7) School of Earth Sciences, Ohio State University, Columbus, OH 43210, USA

[†] Now at Department of Earth and Planetary Sciences, Macquarie University, Sydney, NSW 2109, Australia

* Corresponding author, j.p.odonnell@leeds.ac.uk

Abstract

Accurately monitoring and predicting the evolution of the West Antarctic Ice Sheet via secular changes in the Earth's gravity field requires knowledge of the underlying upper mantle viscosity structure. Published seismic models show the West Antarctic lithosphere to be ~ 70 - 100 km thick and underlain by a low velocity zone extending to at least ~ 200 km. Mantle viscosity is dependent on factors including temperature, grain size, the hydrogen content of olivine, the presence of partial melt and applied stress. As seismic wave propagation is particularly sensitive to thermal variations, seismic velocity provides a means of gauging mantle temperature. In 2012, a magnitude 5.6 intraplate earthquake in Marie Byrd Land was recorded on an array of POLENET-ANET seismometers deployed across West Antarctica. We modeled the waveforms recorded by six of the seismic stations in order to determine realistic estimates of temperature and lithology for the lithospheric mantle beneath Marie Byrd Land and the central West Antarctic Rift System. Published mantle xenolith and magnetotelluric data provided constraints on grain size and hydrogen content, respectively, for viscosity modeling. Considering tectonically-plausible stresses, we estimate that the viscosity of the lithospheric mantle beneath Marie Byrd Land and the central West Antarctic Rift System ranges from $\sim 10^{20} - 10^{22}$ Pa.s. To extend our analysis to the sublithospheric seismic low velocity zone, we used a published shear wave model. We calculated that the velocity reduction observed between the base of the lithosphere (~ 4.4 - 4.7 km/s) and the centre of the low velocity zone (~ 4.2 - 4.3 km/s) beneath West Antarctica could be caused by a 0.1-0.3% melt fraction or a one order of magnitude reduction in grain size. However, the grain size reduction is inconsistent with our viscosity modeling constraints, suggesting that partial melt more feasibly explains the origin of the low velocity zone. Considering plausible asthenospheric stresses, we estimate the viscosity of the seismic low velocity zone beneath West Antarctica to be $\sim 10^{18} - 10^{19}$ Pa.s. It has been shown elsewhere that the inclusion of a low viscosity layer of order 10^{19} Pa.s in Fennoscandian models of glacial isostatic adjustment reduces disparities between predicted surface uplift rates and

30 corresponding field observations. The incorporation of a low viscosity layer reflecting
31 the seismic low velocity zone in Antarctic glacial isostatic adjustment models might
32 similarly lessen the misfit with observed uplift rates.

33 **Key words:** West Antarctica, mantle viscosity, glacial isostatic adjustment, seismic
34 low-velocity zone, seismology

1 Introduction

Warming Circumpolar Deep Water is eroding ice shelves that buttress the West Antarctic Ice Sheet (WAIS) (e.g., Jacobs et al., 2011). The stability of the WAIS is of particular concern because several large outflow glaciers such as Thwaites and Pine Island are thought susceptible to irrevocable ice loss through marine-ice sheet instability (e.g., Joughin et al., 2014). Satellite gravimetry theoretically offers an efficient means of monitoring WAIS mass change and hence quantifying its predicted contribution to sea level rise. In practice, the superimposed gravitational signal of glacial isostatic adjustment (GIA), the slow flow of the Earth’s ductile mantle toward a new equilibrium following the advance or retreat of a significant surface ice load, must first be removed. The viscosity of the mantle means that the adjustment process can lag the instantaneous elastic response of the crust by hundreds or thousands of years. Thus, accurately modeling the GIA process necessitates knowledge of both the ice sheet history and the rheology of the Earth. Both tasks are challenging in a region with limited geological and geophysical data. These limitations are reflected in the disparities between surface uplift rates predicted by GIA models and corresponding field observations (e.g., Thomas et al., 2011).

Progression from the use of global average 1D radial viscosity profiles in GIA modeling to 3D viscosity models informed by global and continental scale seismic tomography models (e.g., van der Wal et al., 2015) has lessened the misfit. As seismic wave propagation is particularly sensitive to thermal variations, and viscosity to temperature, seismic velocity models can help constrain viscosity structure. Recently developed higher resolution seismic models showing crustal and upper mantle heterogeneity beneath West Antarctica can help in this regard. For example, Heeszel et al. (2016) model the West Antarctic lithosphere as being ~ 70 -100 km thick and underlain by a low velocity zone extending to at least ~ 200 km. Such studies circumvent the relative seismic quiescence of the Antarctic continent by relying on teleseismic surface wave and ambient noise analyses to probe the underlying absolute velocity

structure. However, these techniques lend themselves to the determination of shear wave velocity (V_S) structure; compressional wave velocity (V_P) information is generally unforthcoming. This is unfortunate because the combination of V_P and V_S data can further inform rock type and the presence of partial melt, both of which influence viscosity. In 2012, a magnitude 5.6 intraplate earthquake in Marie Byrd Land (MBL) was recorded on an array of POLENET-ANET seismometers deployed across West Antarctica (Figure 1). Many of the seismograms recorded a Pnl wave. This is a long-period body wave observable at regional distance representing a superposition of upper mantle head wave (Pn) and partially trapped crustal (PL) energy (e.g., Helmberger & Engen, 1980). In conjunction with the recorded Rayleigh wave, this afforded us the opportunity to probe the V_P and V_S structure of the crust and uppermost mantle across MBL and the central West Antarctic Rift System (WARS).

In addition to temperature and melt, viscosity also depends on factors such as grain size and the hydrogen content of nominally anhydrous minerals (e.g., Hirth & Kohlstedt, 2003) which are not well constrained across West Antarctica and not so readily extractable from seismic velocity measurements. To this end we combined the seismic information obtained from modeling the MBL earthquake waveforms with magnetotelluric, petrological and mineral physics data to infer realistic values for temperature, grain size, hydrogen content and melt fraction in order to estimate realistic viscosity bounds for the West Antarctic lithospheric mantle. As GIA is thought especially sensitive to upper mantle viscosity structure (e.g., Whitehouse et al., 2012), and because our new seismic model does not extend below the lithosphere, we extended our analysis to the sublithospheric mantle using the shear wave model from Heeszel et al. (2016). We estimated an average viscosity for the central West Antarctic sublithospheric mantle based on the corresponding average velocity structure inferred by Heeszel et al. (2016). The sublithospheric low velocity layer imaged by Heeszel et al. (2016) beneath much of West Antarctica shares many of the attributes of the global seismic low velocity zone (LVZ) that exists beneath most continental areas (Thybo, 2006, and references therein). The global LVZ is generally attributed to either a small

92 amount of partial melt (e.g., Anderson & Spetzler, 1970) or solid-state mechanisms
93 which affect the elastic properties of solid peridotite (e.g., Karato & Jung, 1998). We
94 examined the feasibility of these hypotheses to account for the LVZ beneath West
95 Antarctica and compared them in terms of their viscosity implications.

2 Data and Method

The third International Polar Year 2007-2008 motivated the first deployment of broadband seismometer arrays in the interior of the Antarctic continent. In particular, across West Antarctica an array of seismometers was deployed as part of the POLENET-ANET project (www.polenet.org) to probe the structure of the WARS. The instruments deployed were a mixture of cold-rated Gralp CMG-3T (120s) and Nanometrics T240 (240s) seismometers sampling at 1 and 40 samples per second (sps). 16 of these recorded the June 1st 2012 M5.6 MBL event, an intraplate extensional earthquake estimated to have occurred at a depth of ~ 13 km (Figure 1).

At the given epicentral distances of ~ 175 to 1500 km, the first energy to arrive at the POLENET-ANET seismometers was the Pn seismic phase. This is the portion of the seismic energy that transits the majority of the path between the earthquake hypocenter and seismometer as a compressional head wave in the lithospheric mantle. At these distances, the energy transiting entirely within comparatively lower velocity crustal rock arrived later. The precise arrival time of the Pn wave was readily identifiable on the seismograms and allowed us to infer associated travel times using the hypocenter and origin time reported in the Global Centroid-Moment-Tensor (CMT) catalogue. Analysis of the Pn travel times as a function of epicentral distance points to a consistent regional lithospheric mantle V_P of ~ 7.95 km/s beneath the WARS and MBL (Figure 2). The Sn wave arrival, by comparison, was not reliably identifiable on the seismograms. To extract additional crustal and lithospheric mantle velocity structure information from the earthquake we compared the observed seismograms with synthetic seismograms calculated using the reflection-matrix reflectivity code *mijkennett* (Randall, 1994) for 1D stratified Earth models excited by the reported CMT focal mechanism.

As a preliminary step in the analysis, instrument responses were deconvolved and the observed 1 sps radial- and vertical-component displacement seismograms were

123 then bandpass filtered between 80 and 5 s using a standard Butterworth filter. The
124 5 s cut-off eliminated shorter period content from the seismograms that couldn't be
125 adequately replicated by simple 1D Earth models. The processed seismograms thus
126 encoded the signature of crustal (including the ice layer) and lithospheric mantle
127 structure. In a final step the seismograms were windowed from several seconds before
128 the Pn arrival to several tens of seconds beyond the end of the Rayleigh wave packet,
129 and the amplitudes normalised to the maximum Rayleigh wave amplitude within the
130 respective windows. Aside from the instrument deconvolution, these same steps were
131 applied to the synthetic displacement seismograms to facilitate comparison.

132 We sought synthetic seismograms calculated using *mijkennett* that matched the
133 Pn arrival times and Pnl wave train (if evident) and Rayleigh wave shapes using
134 the statistical concordance coefficient (Lin, 1989) as a metric of wave shape fit. As
135 expected, seismometers located approximately coincident with the earthquake nodal
136 plane recorded little Pnl energy. Conversely, seismometers located off the nodal plane
137 recorded well developed Pnl wave trains. In the former case, fitting the data amounted
138 to matching the Pn phase arrival time and shape of the fundamental mode Rayleigh
139 wave train. In the latter case, the Pnl wave train shape had to be fit in addition.
140 Comparing relative rather than absolute amplitudes made the problem more tractable
141 but precluded us from inferring attenuation values.

142 For each earthquake-seismometer path the 1D Earth structure was parameterised
143 as an ice layer atop a three-layer crust over a lithospheric mantle half-space (see
144 Table 1). The modeled ice layer thicknesses were allowed to vary in accordance with
145 the BEDMAP2 ice thickness estimates (Fretwell et al., 2013) and the ice V_P from
146 3.5 - 4.0 km/s with a fixed V_P/V_S ratio of 1.98 (e.g., Kohnen, 1974). Preceding
147 studies infer crust as thin as ~ 20 km beneath parts of the central WARS and up to
148 ~ 35 km thick beneath MBL (e.g., Chaput et al., 2014; O'Donnell & Nyblade, 2014;
149 Ramirez et al., 2016). As each earthquake-seismometer path samples both domains to
150 differing degrees (Figure 1), we simply required the modeled total crustal thicknesses

151 to lie in the range 22-36 km. Single and two layer crustal parameterisations were
152 initially assessed but found to not fit the observed seismograms to the same degree
153 as three layer crusts. A three-layer parameterisation is additionally in accordance
154 with standard models of continental crustal stratification into upper, mid and lower
155 layers (e.g., Christensen & Mooney, 1995). Incorporation of a seismic LVZ underlying
156 the lithospheric mantle did not improve the waveform fits. As expected, the depth
157 sensitivity of the recorded Rayleigh waves did not extend beyond the lithospheric
158 mantle.

159 The modeled lithospheric mantle V_P was permitted to vary between 7.9 - 8.0 km/s
160 in line with the value estimated from the Pnl travel time analysis, while the litho-
161 spheric mantle V_S range was guided by shear wave velocities of 4.4 - 4.7 km/s inferred
162 in West Antarctica by Heeszel et al. (2016) using teleseismic Rayleigh wave tomogra-
163 phy. For the mid and lower crustal layers, V_P/V_S ratios were allowed vary within the
164 range 1.73 - 1.87 ascribed to continental crust lithologies (e.g., Christensen, 1996).
165 We imposed the additional constraint that the V_P/V_S ratios increase from the mid
166 to lower crust in accordance with the accepted transition to progressively more mafic
167 rock (e.g., Christensen, 1996). By contrast, the upper crustal V_P/V_S ratio was al-
168 lowed to vary independently and within the broader range 1.55 - 1.90 to account
169 for the possibilities of crystalline felsic upper crust lithologies and/or the presence
170 of thick sediment (e.g., Christensen, 1996). An upper mantle V_P/V_S ratio range of
171 1.75 - 1.80 was imposed considering published V_P , V_S and V_P/V_S values for common
172 upper mantle rocks (e.g., Abers & Hacker, 2016, and references therein).

173 To account for potential depth-origin time trade-off in the GCMT solution we per-
174 mitted the reported depth (13.1 km) to vary by ± 4 km when generating synthetic
175 seismograms. Otherwise we assumed the reported focal mechanism to be correct.
176 Young et al. (2012) describe the pitfalls of inadvertently mapping erroneous focal
177 information into velocity structure. The fact that we recover velocity structure con-
178 sistent with seismic models developed independent of this earthquake (Section 3)

lends us confidence that any such inadvertent mapping here is negligible.

It is important to note that we determined vertically-polarised shear wave velocities, V_{SV} , by modeling the Rayleigh waves, and not isotropic velocities, V_S . Isotropic velocities must be calculated from both vertically- and horizontally-polarised wave velocities, either as a pure or weighted average depending on assumptions about the anisotropy. As vertically-polarised shear wave velocities are generally slower than horizontally-polarised counterparts, the V_P/V_S ratios that we infer (more correctly, V_P/V_{SV} ratios) are systematically larger than corresponding isotropic V_P/V_S ratios, probably by about 2%. This systematic bias is not large enough to affect the conclusions drawn from the models. Layer densities, meanwhile, were calculated from the V_P values using an empirical linear velocity-density relationship (Christensen & Mooney, 1995). However, density variations by themselves were found to have a negligible effect on the seismograms in comparison to velocity variations and are not discussed further.

Subject to these considerations, we used *mijkennett* in conjunction with genetic algorithm code *NSGA-II* (Deb et al., 2002) to search for the 1D stratified velocity models best explaining the seismograms for each earthquake-seismometer path. In each case, 60 1D stratified Earth models satisfying the imposed geologic boundary conditions were generated to serve as an initial population for the search algorithm. We found that evolution through 40 subsequent generations (using crossover and mutation probabilities of 0.9 and 0.05, respectively) was sufficient to arrive at the suite of best solutions according to the concordance coefficient metric of waveform similarity. Evolution beyond this yielded no discernible improvements in waveform fitting.

3 Results

3.1 Seismograms

We present 1D velocity models for six of the earthquake-stations paths that yielded concordance coefficients >0.8 for both radial and vertical component seismograms. The paths in question span both the WARS and MBL dome (Figure 1). Figure 3 compares the observed and best fitting synthetic seismograms for these six stations. Station FALL recorded the best-developed Pnl wave train owing to its location with respect to the earthquake epicenter and focal mechanism. Although the Pnl wave train and dominant Rayleigh wave packet are explained reasonably well, the long period energy arriving between 285 - 315 s is poorly fit. It is noteworthy that this portion of the seismogram can be fit if the Pnl constraint is ignored. However, a realistic velocity model should simultaneously explain both the Pnl and Rayleigh wave trains. Thus, we disregard those velocity models which fail to adequately match the Pnl wave train.

Stations WAIS and BYRD also recorded Pnl wave trains, albeit less well-developed than at FALL. In both cases the gross features of the radial and vertical component seismograms are reproduced aside from the higher-frequency oscillations preceding the main Rayleigh wave packet. In contrast, stations DNTW, BEAR and KOLR were located approximately coincident with the nodal plane (see Figure 1) and thus recorded little or no compressional Pnl energy. In these cases, waveform fitting reduces to matching the Rayleigh wave train. In each case the synthetic seismograms re-create the gross features of the recorded seismograms.

3.2 Seismic Velocity Models

Model for paths to stations FALL, WAIS, BYRD and KOLR show lithospheric mantle V_{SV} velocities of ~ 4.4 - 4.5 km/s, while those for DNTW and BEAR show ~ 4.5 - 4.6 km/s (Figure 4). In each case the lithospheric mantle V_P/V_{SV} values are consistent with published values (e.g., Abers & Hacker, 2016, and references therein). The seismic velocities and V_P/V_{SV} values for the mid and lower crustal layers show some spread but generally similarly cluster about values consistent with continental crust averages (e.g., Christensen, 1996). In contrast, the upper crustal layers exhibit large spreads in V_P/V_{SV} values (~ 1.55 - 1.90). This partly reflects the fact that the upper crustal layer velocities parameters were permitted to explore a larger model space than deeper counterparts (Table 1), but also that the shorter period Rayleigh waves (shallow structure) were not fit to the same extent as the longer period Rayleigh waves (deeper structure). This renders the upper crustal layer the least robust part of our velocity models. Consequently we can neither prove nor discount the existence of thick sedimentary layers on the basis of our analysis.

The inferred crustal thicknesses are consistent with the model of relatively thick crust underlying and extending southward from MBL abutting thinner crust characteristic of the WARS (e.g., Chaput et al., 2014). Models for paths predominantly sampling the MBL crustal block (WAIS, BYRD and KOLR) show crustal thicknesses in the range ~ 29 - 33 km, while those for FALL (~ 26 - 28 km), DNTW (~ 23 km) and BEAR (~ 25 - 27 km) show comparatively thinner crust because significant portions of these paths also sample the WARS. While the path average models cannot be compared directly to seismic receiver function point estimates of crustal thickness, the patterns are nonetheless consistent with receiver function data (Ramirez et al., 2016), thickness maps developed from the joint interpretation of receiver functions and ambient noise (Chaput et al., 2014), and receiver functions and gravity data (O'Donnell & Nyblade, 2014). Given the consistency of our crustal models with other studies, we turn our attention to the uppermost mantle and its viscosity structure.

4 Discussion

4.1 Uppermost Mantle Viscosity

For plastic deformation, the effective viscosity, μ_{eff} , characterises the relationship between stress, σ , and strain rate, $\dot{\epsilon}$, according to:

$$\dot{\epsilon} = \mu_{eff}\sigma \quad (1)$$

Subcontinental lithospheric mantle peridotites typically consist of more than 60% volume fraction of olivine, so olivine is commonly regarded as the governing control on upper mantle rheology. Major mechanisms of plastic deformation in olivine are diffusion creep, dislocation creep and dislocation-accommodated grain boundary sliding (DisGBS) (e.g., Hirth & Kohlstedt, 2003; Hansen et al., 2011; Ohuchi et al., 2015). We operate under the assumption that these mechanisms function simultaneously in the upper mantle and that deformation at a point is dominated by the mechanism with the lowest viscosity. For each mechanism, the relationship between stress and strain rate can be formulated as:

$$\dot{\epsilon} = Ad^{-p}C_{OH}^r \exp\left(\frac{E}{RT}\right)\sigma^n, \quad (2)$$

where A is a pre-exponential factor, d is grain size, p is the grain size exponent, C_{OH} is water (hydrogen) content, r is the water exponent, E is activation enthalpy, R is the gas constant, T is absolute temperature and n is the stress exponent (e.g., Hirth & Kohlstedt, 2003). If the applied stress is known, a combination of laboratory rheological data and geophysical field observations can be used to constrain the values of the various parameters in Equation 2 and thus infer the effective viscosity of the upper mantle.

Lithospheric differential stress magnitudes are generally thought to range from ~ 10 – 100 MPa (Ghosh & Holt, 2012). Shear stresses acting at the base of slabless tectonic plates are thought not to exceed 1 MPa (e.g., Bird et al., 2008). In particular, by modeling and iteratively adjusting the stresses acting on each tectonic plate to match

observed plate velocities Bird et al. (2008) suggest that a mean shear stress of 0.1 MPa acts at the base of the Antarctic plate. Meanwhile, a representative stress range up to order 10 MPa associated with ice sheet growth and decay has been suggested by a geodynamic study examining the enhancement of volcanism and geothermal heat flux by ice-age cycling in Greenland (Stevens et al., 2016).

In what follows we combine seismic, magnetotelluric, petrological and mineral physics data to infer plausible temperature, grain size and water content ranges for both the lithospheric mantle and sublithospheric uppermost mantle beneath West Antarctica. The inferred temperature, grain size and water content ranges are then inserted in Equation 2 in order to estimate effective viscosity ranges for the lithospheric mantle and sublithospheric uppermost mantle beneath West Antarctica. Rheological parameters for diffusion creep, dislocation creep and DisGBS regimes in Equation 2 are taken from Hirth & Kohlstedt (2003), Hansen et al. (2011) and Ohuchi et al. (2015) ($p=3$, $r=0.8$, $n=1$ for diffusion creep; $p=0$, $r=1.2$, $n=3.5$ for dislocation creep; $p=1$, $r=1.25$, $n=3$ for DisGBS).

4.1.1 The Lithospheric Mantle

Hammond & Humphreys (2000) calculated that seismic V_P and V_S reductions per percent partial melt will be at least 3.6% and 7.9%, respectively, accompanied by a pronounced increase in the V_P/V_S ratio. Recent seismic tomography studies of the broader WARS attributed seismic velocity anomalies to thermal variations within the upper mantle (e.g., Lloyd et al., 2015; Heeszel et al., 2016) without recourse to melt. Furthermore, the lithospheric mantle V_P/V_S ratios obtained in the present study are consistent with typical melt-free lithospheric mantle. We do not discount the fact that pockets of melt may be present in the lithospheric mantle of West Antarctica; numerous active and relict magmatic complexes have been identified (e.g., Lough et al., 2013) and high heat flow measurements have been reported at ice-core drill sites (e.g. 285 ± 80 mW/m² at Subglacial Lake Whillans; Fisher et al., 2015). However, the seismic data suggest that if melting is occurring in the West Antarctic lithospheric mantle, it is localised rather than pervasive and therefore not a dominant influence on the regional viscosity structure.

Conductive anomalies can likewise be caused by melt or fluids, but the conductivity of melt-free lithospheric mantle is controlled by temperature and the hydrogen content of nominally anhydrous minerals (Selway, 2014). Magnetotelluric data indicate a relatively resistive lithospheric mantle beneath the Byrd Subglacial Basin of the central WARS, which Wannamaker et al. (1996) interpreted as reflecting a dormant state of rifting. According to laboratory experiments on the dependence of the conductivity of olivine on water content at upper mantle conditions (Gardés et al., 2014), the 3000 Ohm m resistivity inferred by Wannamaker et al. (1996) for the lithospheric mantle can be explained by dry olivine. Thus, the survey points not only to an absence of melt and fluid, but to a negligible hydrogen content locally in the uppermost mantle beneath the Byrd Subglacial Basin. However, we will also consider a typical “wet” rheology (100 wt ppm H₂O, e.g., Selway, 2014) in case the Byrd Subglacial Basin is not representative of the broader WARS.

Based on data from 60 mineral end-members, Abers & Hacker (2016) provide software for calculating seismic velocities of crustal and mantle rocks at temperature and pressure conditions relevant to the upper few hundreds of kilometers of the Earth. Alternatively, temperature can be inferred at a given pressure if rock composition and seismic velocity are known. A spinel peridotite xenolith suite from Marie Byrd Land described in Handler et al. (2003) serves as a compositional guide to the regional West Antarctic lithospheric mantle. We used Abers & Hacker (2016) to infer a plausible lithospheric mantle temperature range at ~ 50 km depth by matching predicted and observed V_P values for similar peridotitic rock compositions at a pressure of 1.5 GPa. The V_P range inferred in this study, ~ 7.9 -8.0 km/s, translates to a temperature bracket of ~ 800 -1000°C at ~ 50 km depth. This is in agreement with lithospheric mantle temperatures inferred from xenoliths in other regions which have undergone Phanerozoic tectonism (Artemieva, 2006, and references therein). Handler et al. (2003) report the xenolith textures as ranging from fine to coarse. In the viscosity calculations we vary the grain size from 0.1-10 mm to encompass grain sizes typically observed in lithospheric mantle xenoliths worldwide. Taking these considerations into account, using Equation 2 we calculated the effective viscosity of the lithospheric mantle as a function of temperature, grain size and representative lithospheric stresses of 1, 10 and 100 MPa for both dry (0 wt ppm H₂O) and wet (100 wt ppm H₂O) conditions (Figure 5). For both dry and wet compositions, the effect of grain size reduction on viscosity is most pronounced at small stresses: a grain size reduction of one order of magnitude leads to an approximately two to three orders of magnitude viscosity reduction at 1 MPa, but less than an order of magnitude viscosity reduction at 100 MPa. At all stress levels, dry olivine is, as expected, more viscous than wet olivine. The 200°C temperature uncertainty translates to a three to five orders of magnitude variation in viscosity. Considering only those solutions giving tectonically plausible strain rates ($10^{-16} - 10^{-14}$ /s, e.g. Turcotte & Schubert, 2002), the viscosity of dry lithospheric mantle is $\sim 10^{21} - 10^{22}$ Pa s and the viscosity of wet lithospheric mantle is $\sim 10^{20} - 10^{22}$ Pa s. This is in good agreement with experimental analysis based on the Oman Ophiolite (Homburg et al., 2010) and global geodynamic

350 models (e.g., Ghosh & Holt, 2012).

4.1.2 The Sublithospheric Mantle

Because the seismic models developed in this study do not constrain the velocity structure of the sublithospheric mantle, we use the seismic model of Heeszel et al. (2016) to estimate the viscosity of the upper mantle directly beneath the lithosphere. Heeszel et al. (2016) imaged seismically fast lithospheric mantle V_{SV} velocities with magnitudes consistent with the results of this study extending to 70-100 km depth beneath West Antarctica, underlain by slower V_{SV} velocities of ~ 4.2 - 4.3 km/s extending to depths of at least 180 km. This represents a V_S reduction in the range ~ 2 - 9% . Heeszel et al. (2016) interpret the slow shear wave velocities as representing thermally perturbed mantle from Mesozoic through Cenozoic extension in the WARS. Lloyd et al. (2015) similarly interpret relative reductions in V_P and V_S velocities beneath the Bentley Subglacial Trench of the central WARS as reflecting a thermal anomaly consistent with Neogene extension. Both studies attribute seismic velocity reductions beneath MBL to an upper mantle thermal anomaly conceivably related to a putative mantle plume.

The seismic velocity and thickness (70-100 km) of the lithosphere inferred by our work and Heeszel et al. (2016) indicate little broad-scale modification of the uppermost mantle from Cenozoic tectonism. In addition, the low velocity layer imaged by Heeszel et al. (2016) in the sublithospheric mantle beneath much of West Antarctica, on average, shares many of the attributes of the global seismic low velocity zone (Thybo, 2006, and references therein). In what follows we investigate the rheological implications of the average velocity structure of the central West Antarctic sublithospheric mantle. In doing so we neglect localised velocity variations rooted in Cenozoic tectonism (e.g., Lloyd et al., 2015) that will play an important role in 3D viscosity analyses.

Although still a matter of debate, the origin of the LVZ is generally attributed to either a small amount of partial melt (e.g., Anderson & Spetzler, 1970) or solid-state

mechanisms which affect the elastic properties of solid peridotite (e.g., Karato & Jung, 1998). Chantel et al. (2016) suggest that 0.1 to 0.3% melt fractions are consistent with seismic, electrical conductivity and petrological observations, and that partial melt is a viable physical origin for the LVZ. Models of solid-state mechanisms such as grain size evolution successfully replicate many of the observed seismic signatures of the upper mantle (e.g., Behn et al., 2009). However, in contrast to melt, solid-state explanations generally struggle to explain the sharp velocity drop at the top of the LVZ (e.g., Stixrude & Lithgow-Bertelloni, 2005). Elastically accommodated grain-boundary sliding (EAGBS; Raj & Ashby, 1971) causes a frequency, temperature, and grain-size dependent peak in seismic attenuation and may be a solid-state candidate capable of producing the observed sharp gradient in velocity (e.g., Karato, 2012). In what follows, we examine the implications of the partial melt and EAGBS hypotheses for the viscosity of the LVZ beneath West Antarctica.

We estimate the temperature difference between the lithosphere and the LVZ by assuming a mantle potential temperature of $\sim 1300\text{--}1450^\circ\text{C}$ (e.g., O'Reilly & Griffin, 2010) and an upper mantle adiabat of $0.4\text{--}0.5^\circ\text{C}/\text{km}$ (Katsura et al., 2010). Taking 85 km as a reasonable average lithospheric thickness for West Antarctica (Heeszel et al., 2016), these values translate to temperature estimates of $\sim 1340\text{--}1490^\circ\text{C}$ at the lithosphere-asthenosphere boundary (LAB) and $\sim 1360\text{--}1515^\circ\text{C}$ at a depth of 125 km in the center of the LVZ.

398 Velocity reduction due to partial melt

399 Partial melting of dry peridotite will only begin to occur at $\sim 1570^\circ\text{C}$ at 125 km
400 depth (~ 4 GPa) (Hirschmann et al., 2009). However, asthenospheric peridotite is
401 likely to contain 100-500 ppm hydrogen, which would lower its solidus in the LVZ
402 to a temperature below the geotherm (e.g., Hirschmann et al., 2009; Ardia et al.,
403 2012, and references therein) and produce melt fractions of the order of 0.1-0.3%
404 (Hirschmann et al., 2009). A melt fraction of this magnitude would cause the V_S
405 velocity reduction (~ 4.4 - 4.7 km/s to ~ 4.2 - 4.3 km/s) observed in the LVZ below West
406 Antarctica (Chantel et al., 2016).

407 Figure 6 shows the hydrogen content necessary to generate melt at our calculated
408 range of LVZ temperatures at 125 km depth (1360, 1435 and 1515°C). At 1360°C ,
409 melting will not initiate unless the peridotite contains at least ~ 490 ppm hydrogen
410 and a melt fraction of 0.1-0.3% will not be generated unless the hydrogen content
411 reaches ~ 580 - 800 ppm. These hydrogen contents approach and exceed the estimated
412 peridotite hydrogen storage capacity at this depth (e.g., Ardia et al., 2012). At the
413 higher estimated temperatures of 1435 and 1515°C , physically plausible hydrogen
414 contents of ~ 285 ppm and ~ 115 ppm will initiate melting while melt fractions of 0.1-
415 0.3% will be generated for hydrogen contents of ~ 340 - 470 ppm and ~ 140 - 190 ppm,
416 respectively.

417 **Velocity reduction due to EAGBS**

418 Since grain size affects both viscosity and seismic velocity, we considered whether
419 grain size reduction could be a solid-state cause for the LVZ. We used the experimental
420 results summarised in Jackson et al. (2014) to calculate the predicted change in shear
421 wave velocity due to EAGBS between 85 km depth (at the base of the lithosphere;
422 ~ 1340 - 1490°C) and 125 km depth (in the center of the LVZ; ~ 1360 - 1515°C) for grain
423 sizes between 0.1 and 10 mm. Figure 7 shows that while EAGBS is unlikely to
424 account for the seismic observations if grain size does not vary between these depths,
425 a reduction in grain size of one order of magnitude can produce a velocity decrease
426 that matches the seismic observations.

Viscosity implications of the partial melt and EAGBS LVZ hypotheses

For small melt fractions, ϕ , several constitutive equations relating the viscosity of partially-molten rock, $\mu(\phi)$, to its melt-free counterpart, μ_0 , have been proposed. Experimentalists suggest that viscosity decreases exponentially with increasing melt fraction according to:

$$\mu(\phi) = e^{-\alpha\phi}\mu_0, \quad (3)$$

where $\alpha \approx 26$ for diffusion creep and $\alpha \approx 31$ for dislocation creep (e.g., Hirth & Kohlstedt, 2003). Meanwhile, Takei & Holtzman (2009) derived a theoretical formulation:

$$\mu(\phi) = 0.2(1 - A\phi^{1/2})^2\mu_0, \quad (4)$$

where $A = 2.3$ is a semi-empirically determined constant, while Holtzman (2016) developed a parameterisation for very small ($< 1\%$) melt fractions:

$$\mu(\phi) = \exp(-(\alpha\phi + \ln x_{\phi_c} \operatorname{erf}(\phi/\phi_c)))\mu_0, \quad (5)$$

where x_{ϕ_c} is the viscosity reduction factor at the critical melt fraction, ϕ_c , and $\alpha \approx 26$. According to the experimental formulation of Equation 3, melt fractions of 0.1-0.3% will reduce the viscosity of partially-molten rock relative to the melt-free counterpart by a factor of ~ 1.02 - 1.09 . For the same melt fractions, the theoretical formulations of Equations 4 and 5 (taking $x_{\phi_c} = 120$ and $\phi_c = 10^{-5}$ as suggested for peridotite) result in viscosity reduction factors of ~ 5.8 - 6.5 and ~ 123 - 130 , respectively.

Using Equation 2 we calculated the effective viscosity of the LVZ beneath West Antarctica for anhydrous and water-saturated peridotite as a function of temperature, grain size and stress (Figure 8). We then used Equations 3, 4 and 5 to calculate the viscosity for a melt fraction of 0.1% for the respective viscosity-melt formulations (Figure 9). The applied stress range of 0.1-10 MPa considered encompasses the superposition of an assumed mean basal shear stress of 0.1 MPa (Bird et al., 2008) and a representative stress range associated with ice sheet growth and decay (up to 10 MPa; Stevens et al., 2016). Several broad trends are apparent from Figures 8 and 9. The

effect of grain size reduction on viscosity is very large for small stresses but becomes negligible at large stresses. This is due to the transition from the grain-size sensitive diffusion creep regime at low stresses towards the grain-size insensitive dislocation creep regime at higher stresses. Our 150°C temperature uncertainty has a larger apparent effect on the viscosity of anhydrous peridotite compared to water-saturated or partially molten peridotites. However, temperature has secondary impacts on viscosity for wet conditions, particularly in that it controls the amount of hydrogen required to saturate and melt peridotite. At all stress levels, the anhydrous peridotite has the highest viscosity, while the calculated reduction in viscosity due to partial melt depends on the constitutive equation used.

We constrain our set of solutions by considering only those giving plausible asthenospheric strain rates ($10^{-16} - 10^{-14}$ /s, e.g. Turcotte & Schubert, 2002). For stresses of 0.1 to 10 MPa, these strain rates translate to viscosities ranging from $\sim 10^{18} - 10^{20}$ MPa. Within our modelled range of compositions and stresses, these viscosities are only realisable for a grain size of 10 mm and a stress of 0.1 MPa (Figures 8 and 9). The 0.1 MPa stress level suggests that asthenospheric stresses associated with GIA are of the same order of magnitude as stresses acting on the base of the Antarctic plate due to mantle convection (~ 0.1 MPa; Bird et al., 2008).

Figure 7 showed that a grain size reduction of one order of magnitude from the base of the lithosphere would be necessary for EAGBS to explain the LVZ. Given that we can only model plausible LVZ strain rates for grain sizes equal to (or larger than) lithospheric mantle counterparts (Figure 5), our analysis does not support grain size reduction as a means of explaining the LVZ. For West Antarctica, the 0.1 to 0.3% melt fractions that viably explain the LVZ seismically translate to a viscosity of $\sim 10^{18} - 10^{19}$ Pa s for a 10 mm grain size at 0.1 MPa according to the formulation of Hirth & Kohlstedt (2003) (Equation 3). According of the theoretical formulation of Takei & Holtzman (2009) (Equation 4), a 0.1% melt fraction gives a viscosity of $\sim 10^{18}$ Pa s for a 10 mm grain size and stress of 0.1 MPa at 1360°C. However, we

479 have previously commented that the hydrogen content required to generate such
480 a melt fraction at this temperature approaches the estimated peridotite hydrogen
481 storage capacity for the estimated depth (e.g., Ardia et al., 2012). The formulation
482 of Holtzman (2016) (Equation 5), meanwhile, results in implausibly low strain rates
483 for all considered scenarios. Within the limitations of our analysis, this suggests
484 that the partial melt hypothesis for the origin of the seismic LVZ is feasible only if
485 the associated viscosity reduction is of the magnitude suggested by the formulations
486 of Hirth & Kohlstedt (2003), and perhaps Takei & Holtzman (2009). Taking these
487 considerations into account, the viscosity of $\sim 10^{18} - 10^{19}$ Pa s inferred for plausible
488 strain rates is in broad agreement with van der Wal et al. (2015) who determined that
489 West Antarctic uppermost mantle viscosities may in places be less than 10^{19} Pa s. In
490 comparison, the volume-averaged viscosity of the upper mantle is thought to be of
491 order 10^{20} Pa s (e.g., Kaufmann & Lambeck, 2002).

492 Much of what we know about GIA and mantle viscosity comes from studies of
493 Fennoscandia and North America. In fact, the comparative paucity of Antarctic data
494 means that Antarctic GIA models are typically calibrated against northern hemi-
495 sphere data sets (e.g., van der Wal et al., 2015). Fennoscandia and much of North
496 America are shield regions: the lithosphere is thick, cold, buoyant and stable. West
497 Antarctica, by comparison, is an amalgamation of several terranes that have witnessed
498 significant tectonic deformation and re-organisation since the breakup of Gondwana.
499 The upper mantle velocity structure, and hence anticipated thermal and viscosity
500 structure, of the respective regions is markedly different.

501 Fjeldskaar (1994) argued that Fennoscandian GIA models including a low viscosity
502 asthenospheric layer of order 10^{19} Pa s better explain observed surface uplift rates than
503 models lacking this layer. The incorporation of a low viscosity layer ($\sim 10^{18} - 10^{19}$ Pa s)
504 reflecting the seismic LVZ in Antarctic GIA models might similarly improve the fit to
505 surface observables used to validate the GIA models. However, care should be taken
506 if Antarctic GIA models including a sublithospheric low viscosity layer models are

507 calibrated against northern hemisphere data sets: the LVZ beneath shield regions is
508 considerably thinner than it is beneath actively deforming regions (Thybo, 2006).

509 Surface Heat Flow

510 Another crucial factor influencing ice sheet behaviour, the average heat flow at the ice
511 sheet base, can similarly be estimated from seismic models. Based on a compilation
512 of global data, Artemieva (2006) suggests that a correlation between depth to the
513 upper mantle high-conductivity layer, Z_{HCL} , (interpreted as electrically conductive
514 asthenosphere) and surface heat flow, Q , can be approximated as:

$$Z_{HCL} = 418 \times e^{-0.023 Q} \quad (6)$$

515 While acknowledging that seismic and electrical lithospheres need not coincide, a
516 lithospheric thickness range of 70-100 km in Equation 6 translates to a surface heat
517 flow of $\sim 62 - 78 \text{ mW/m}^2$. Such a range may better represent the average heat flow of
518 West Antarctica than locally elevated measurements such as $285 \pm 80 \text{ mW/m}^2$ inferred
519 at Subglacial Lake Whillans (Fisher et al., 2015). Heeszel et al. (2016) and Ramirez
520 et al. (2016) draw similar conclusions from their seismic analyses.

5 Conclusion

Accurately estimating the upper mantle viscosity structure of West Antarctica is a critical aspect of the monitoring and prediction of West Antarctic Ice Sheet evolution by satellite gravimetry. As both seismic wave propagation and viscosity are particularly sensitive to thermal variations, seismic data can provide useful constraints on mantle viscosity. We utilised seismograms from the 2012, magnitude 5.6, intraplate earthquake in Marie Byrd Land to obtain V_P and V_S data for West Antarctica. While thermal variations can be estimated from V_S (or V_P) alone, the additional V_P/V_S information informs rock type and the presence of partial melt, both of which influence viscosity. We used a genetic algorithm to converge on a population of path-average crustal and uppermost mantle velocity models best explaining the observed seismograms at six POLENET-ANET stations. Inferred crustal thicknesses are consistent with the concept of relatively thick crust underlying and extending southward from MBL abutting thinner crust characteristic of the WARS. Models for paths predominantly sampling the MBL crustal block (WAIS, BYRD and KOLR) show crustal thicknesses in the range ~ 29 - 33 km, while those for FALL (~ 26 - 28 km), DNTW (~ 23 km) and BEAR (~ 25 - 27 km) show comparatively thinner crust because significant portions of these paths also sample the WARS. V_P/V_S values for the mid and lower crustal layers generally cluster about values consistent with continental crust averages. The inferred uppermost mantle seismic velocities are consistent with melt-free peridotite. We combined the seismic information with petrological and magnetotelluric data to examine the rheology of the West Antarctic lithospheric mantle. For realistic differential stresses of 1-100 MPa and tectonically plausible strain rates of $10^{-16} - 10^{-14}$ /s, the lithospheric mantle viscosity ranges from $\sim 10^{20} - 10^{22}$ Pa.s. Furthermore, if the West Antarctic lithosphere is 70-100 km thick as suggested by Heeszel et al. (2016), a correlation between depth to the asthenosphere and surface heat flow postulated by Artemieva (2006) suggests that $\sim 62 - 78$ mW/m² may represent the average surface heat flow of West Antarctica.

To extend our analysis to the sublithospheric mantle, we used the shear wave model from Heeszel et al. (2016). We calculated that the velocity reduction observed between the base of the lithosphere and the centre of the LVZ beneath West Antarctica could be caused by a 0.1-0.3% melt fraction (Chantel et al., 2016) or a one order of magnitude reduction in grain size (Jackson et al., 2014). For plausible asthenospheric stresses of 0.1-10 MPa and strain rates of $10^{-16} - 10^{-14}$ /s, the viscosity of the LVZ is $\sim 10^{18} - 10^{20}$ Pa.s. Fjeldskaar (1994) showed that the incorporation of a low viscosity asthenospheric layer of order 10^{19} Pa.s in Fennoscandian GIA models improved matches to surface observations. Notably our inferred viscosities are only realisable for a grain size of 10 mm and a stress of 0.1 MPa.

Our results have important implications for the stress level of the asthenosphere and the cause of the LVZ. Estimates for realistic asthenospheric strain rates can only be replicated for low stresses (< 1 MPa). This implies that, if these estimates are valid for asthenosphere affected by GIA, asthenospheric stresses associated with GIA are of the same order of magnitude as stresses acting on the base of the Antarctic plate due to mantle convection. These asthenospheric strain rates can also only be replicated for coarse grain sizes (~ 10 mm). This implies that the seismic velocity decrease observed in the LVZ cannot be caused by a solid state mechanism (EAGBS) responding to a grain-size reduction in this zone, suggesting that partial melt is more likely responsible for the LVZ. That said, we argue that the partial melt hypothesis is only valid if the viscosity reduction associated with a 0.1-0.3% melt fraction is relatively modest, in line with the formulations of Hirth & Kohlstedt (2003) and, under certain conditions, Takei & Holtzman (2009). Formulations which infer larger viscosity reductions (e.g., Holtzman, 2016) give implausibly low strain rates for the conditions considered. Interestingly, the vast majority of our models for reasonable sublithospheric compositions, grain-sizes and stresses (Figure 7) produce viscosities significantly lower than those generally predicted from GIA studies (e.g., Kaufmann & Lambeck, 2002). Figure 8 demonstrates the large influence hydrogen exerts on sublithospheric mantle viscosity. If the initiation of partial melting leads to a decrease

578 in peridotite hydrogen content below its water-saturated level, it is conceivable that
579 partial melting could result in an actual increase in viscosity. Since most of the
580 modelled compositions have viscosities too low to match the observations, a LVZ
581 with a small degree of partial melt and an associated decrease in peridotite hydrogen
582 content will broaden the range of parameters that can reconcile the seismic, viscosity,
583 grain size and stress constraints.

6 Acknowledgements

We would like to acknowledge the support of all the field teams associated with the POLENET-ANET project. We thank the pilots of Kenn Borek Air and the New York Air Guard for flight support and field camp staff for logistical support. POLENET-ANET is supported by NSF Office of Polar Programs grants 0632230, 0632239, 0652322, 0632335, 0632136, 0632209, and 0632185. Seismic instrumentation is provided and supported by the Incorporated Research Institutions for Seismology (IRIS) through the PASSCAL Instrument Center. The POLENET-ANET seismic data can be accessed through the IRIS Data Management Center (<http://www.iris.edu/mda>). The facilities of the IRIS Consortium are supported by the NSF under cooperative agreement EAR-1063471, the NSF Office of Polar Programs, and the DOE National Nuclear Security Administration. Anya M. Reading and another reviewer provided thoughtful reviews which improved the clarity of this paper.

References

- Abers, G. A. & Hacker, B. R., 2016. A MATLAB toolbox and Excel workbook for calculating the densities, seismic wave speeds, and major element composition of minerals and rocks at pressure and temperature, *Geochem. Geophys. Geosyst.*, **17**(2), 616–624, doi:10.1002/2015GC006171.
- Anderson, D. L. & Spetzler, H., 1970. Partial melting and the low-velocity zone, *Phys. Earth Planet. Int.*, **4**(1), 62–64, doi:10.1016/0031-9201(70)90030-0.
- Ardia, P., Hirschmann, M. M., Withers, A. C., & Tenner, T. J., 2012. H₂O storage capacity of olivine at 5-8GPa and consequences for dehydration partial melting of the upper mantle, *Earth Planet. Sci. Lett.*, **345**, 104–116.
- Artemieva, I. M., 2006. Global 1° x 1° thermal model TC1 for the continental lithosphere: Implications for lithosphere secular evolution, *Tectonophysics*, **416**(1-4), 245–277, doi:10.1016/j.tecto.2005.11.022.
- Behn, M. D., Hirth, G., & Elsenbeck II, J. R., 2009. Implications of grain size evolution on the seismic structure of the oceanic upper mantle, *Earth Planet. Sci. Lett.*, **282**(1), 178–189.
- Bird, P., Liu, Z., & Rucker, W. K., 2008. Stresses that drive the plates from below: Definitions, computational path, model optimization, and error analysis, *J. Geophys. Res.*, **113**(B11), doi:10.1029/2007JB005460.
- Chantel, J., Manthilake, G., Andraut, D., Novella, D., Yu, T., & Wang, Y., 2016. Experimental evidence supports mantle partial melting in the asthenosphere, *Sci. Adv.*, **2**(5), doi:10.1126/sciadv.1600246.
- Chaput, J., Aster, R. C., Huerta, A., Sun, X., Lloyd, A., Wiens, D., Nyblade, A., Anandakrishnan, S., Winberry, J. P., & Wilson, T., 2014. The Crustal Thickness of West Antarctica, *J. Geophys. Res.*, **119**, 1–18, doi:10.1002/2013JB010642.

- Christensen, N. I., 1996. Poisson's ratio and crustal seismology, *J. Geophys. Res.*, **101**(B2), 3139–3156, doi:10.1029/95JB03446.
- Christensen, N. I. & Mooney, W. D., 1995. Seismic velocity structure and composition of the continental crust: A global view, *J. Geophys. Res.*, **100**(B6), 9761–9788.
- Deb, K., Pratap, A., Agarwal, S., & T. Meyarivan, T., 2002. A fast and elitist multiobjective genetic algorithm: NSGA-II, *IEEE Trans. Evol. Comp.*, **6**(2), 182–197.
- Fisher, A. T., Mankoff, K. D., Tulaczyk, S. M., Tyler, S. W., Foley, N., & the WISSARD science team, 2015. High geothermal heat flux measured below the West Antarctic Ice Sheet, *Sci. Adv.*, **1**(6), doi:10.1126/sciadv.1500093.
- Fjeldskaar, W., 1994. Viscosity and thickness of the asthenosphere detected from the Fennoscandian uplift, *Earth Planet. Sci. Lett.*, **126**(4), 399–410, doi:10.1016/0012-821X(94)90120-1.
- Fretwell, P., Pritchard, H. D., Vaughan, D. G., Bamber, J. L., Barrand, N. E., Bell, R., Bianchi, C., Bingham, R. G., Blankenship, D. D., Casassa, G., Catania, G., Callens, D., Conway, H., Cook, A. J., Corr, H. F. J., Damaske, D., Damm, V., Ferraccioli, F., Forsberg, R., Fujita, S., Gim, Y., Gogineni, P., Griggs, J. A., Hindmarsh, R. C. A., Holmlund, P., Holt, J. W., Jacobel, R. W., Jenkins, A., Jokat, W., Jordan, T., King, E. C., Kohler, J., Krabill, W., Riger-Kusk, M., Langley, K. A., Leitchenkov, G., Leuschen, C., Luyendyk, B. P., Matsuoka, K., Mouginot, J., Nitsche, F. O., Nogi, Y., Nost, O. A., Popov, S. V., Rignot, E., Rippin, D. M., Rivera, A., Roberts, J., Ross, N., Siegert, M. J., Smith, A. M., Steinhage, D., Studinger, M., Sun, B., Tinto, B. K., Welch, B. C., Wilson, D., Young, D. A., Xiangbin, C., & Zirizzotti, A., 2013. Bedmap2: improved ice bed, surface and thickness datasets for Antarctica, *The Cryosphere*, **7**, 375–393, doi:10.5194/tc-7-375-2013.
- Gardés, E., Gaillard, F., & Tarits, P., 2014. Toward a unified hydrous olivine electrical conductivity law, *Geochem. Geophys. Geosyst.*, **15**(12), 4984–5000, doi:10.1002/2014GC005496.

- Ghosh, A. & Holt, W. E., 2012. Plate Motions and Stresses from Global Dynamic Models, *Science*, **335**(6070), 838–843, doi:10.1126/science.1214209.
- Hammond, W. C. & Humphreys, E. D., 2000. Upper mantle seismic wave velocity: Effects of realistic partial melt geometries, *J. Geophys. Res.*, **105**(B5), 10975–10986.
- Handler, M. R., Wysoczanski, R. J., & Gamble, J. A., 2003. Proterozoic lithosphere in Marie Byrd Land, West Antarctica: Re-Os systematics of spinel peridotite xenoliths, *Chem. Geol.*, **196**(1-4), 131–145, doi:10.1016/S0009-2541(02)00410-2.
- Hansen, L. N., Zimmerman, M. E., & Kohlstedt, D. L., 2011. Grain boundary sliding in San Carlos olivine: Flow law parameters and crystallographic-preferred orientation, *J. Geophys. Res.*, **116**(B8), doi:10.1029/2011JB008220.
- Heeszel, D. S., Wiens, D. A., Anandakrishnan, S., Aster, R. C., Dalziel, I. W. D., Huerta, A. D., Nyblade, A. A., Wilson, T. J., & Winberry, P., 2016. Upper mantle structure of central and West Antarctica from array analysis of Rayleigh wave phase velocities, *J. Geophys. Res.*, doi:10.1002/2015JB012616.
- Helmberger, D. V. & Engen, G. R., 1980. Modeling the long-period body waves from shallow earthquakes at regional ranges, *Bull., Seis. Soc. Am.*, **70**(5), 1699–1714.
- Hirschmann, M. M., Tenner, T., Aubaud, C., & Withers, A. C., 2009. Dehydration melting of nominally anhydrous mantle: The primacy of partitioning, *Phys. Earth Planet. Int.*, **176**(1), 54–68.
- Hirth, G. & Kohlstedt, D., 2003. Rheology of the Upper Mantle and the Mantle Wedge: A View from the Experimentalists, in Inside the Subduction Factory, pp. 83–105, ed. Eiler, J., American Geophysical Union, doi:10.1029/138GM06.
- Holtzman, B. K., 2016. Questions on the existence, persistence, and mechanical effects of a very small melt fraction in the asthenosphere, *Geochem. Geophys. Geosyst.*, **17**(2), 470–484, doi:10.1002/2015GC006102.

- Homburg, J. M., Hirth, G., & Kelemen, P. B., 2010. Investigation of the strength contrast at the Moho: A case study from the Oman Ophiolite, *Geology*, **38**(8), 679–682.
- Jackson, I., Faul, U. H., & Skelton, R., 2014. Elastically accommodated grain-boundary sliding: New insights from experiment and modeling, *Phys. Earth Planet. Int.*, **228**, 203–210, doi:10.1016/j.pepi.2013.11.014.
- Jacobs, S. S., Jenkins, A., Giulivi, C. F., & Dutrieux, P., 2011. Stronger ocean circulation and increased melting under Pine Island Glacier ice shelf, *Nat. Geosci.*, **4**(8), 519–523.
- Joughin, I., Smith, B. E., & Medley, B., 2014. Marine Ice Sheet Collapse Potentially Under Way for the Thwaites Glacier Basin, West Antarctica, *Science*, **344**(6185), 735–738, doi:10.1126/science.1249055.
- Karato, S.-I., 2012. On the origin of the asthenosphere, *Earth Planet. Sci. Lett.*, **321-322**, 95–103, doi:10.1016/j.epsl.2012.01.001.
- Karato, S.-I. & Jung, H., 1998. Water, partial melting and the origin of the seismic low velocity and high attenuation zone in the upper mantle, *Earth Planet. Sci. Lett.*, **157**, 193–207.
- Katsura, T., Yoneda, A., Yamazaki, D., Yoshino, T., & Ito, E., 2010. Adiabatic temperature profile in the mantle, *Phys. Earth Planet. Int.*, **183**(1-2), 212–218, doi:10.1016/j.pepi.2010.07.001.
- Kaufmann, G. & Lambeck, K., 2002. Glacial isostatic adjustment and the radial viscosity profile from inverse modeling, *J. Geophys. Res.*, **107**(B11), ETG 5–1–ETG 5–15, doi:10.1029/2001JB000941.
- Kohnen, H., 1974. The temperature dependence of seismic waves in ice, *J. Glaciol.*, **13**(67), 144–147.

- Lin, L. I.-K., 1989. A Concordance Correlation Coefficient to Evaluate Reproducibility, *Biometrics*, **45**(1), 255–268.
- Lloyd, A. J., Wiens, D. A., Nyblade, A. A., Anandakrishnan, S., Aster, R. C., Huerta, A. D., Wilson, T. J., Dalziel, I. W. D., Shore, P. J., & Zhao, D., 2015. A seismic transect across West Antarctica: Evidence for mantle thermal anomalies beneath the Bentley Subglacial Trench and the Marie Byrd Land Dome, *J. Geophys. Res.*, **120**(12), 8439–8460, doi:10.1002/2015JB012455.
- Lough, A. C., Wiens, D. A., Barcheck, C. G., Anandakrishnan, S., Aster, R. C., Blankenship, D. D., Huerta, A. D., Nyblade, A., Young, D. A., & Wilson, T. J., 2013. Seismic detection of an active subglacial magmatic complex in Marie Byrd Land, Antarctica, *Nat. Geosci.*, **6**(12), 1031–1035.
- O'Donnell, J. P. & Nyblade, A. A., 2014. Antarctica's hypsometry and crustal thickness: Implications for the origin of anomalous topography in East Antarctica, *Earth Planet. Sci. Lett.*, **388**, 143–155.
- Ohuchi, T., Kawazoe, T., Higo, Y., Funakoshi, K.-I., Suzuki, A., Kikegawa, T., & Irifune, T., 2015. Dislocation-accommodated grain boundary sliding as the major deformation mechanism of olivine in the Earth's upper mantle, *Sci. Adv.*, **1**(9), e1500360.
- O'Reilly, S. Y. & Griffin, W. L., 2010. The continental lithosphere-asthenosphere boundary: Can we sample it?, *Lithos*, **120**(1-2), 1–13, doi:10.1016/j.lithos.2010.03.016.
- Raj, R. & Ashby, M. F., 1971. On grain boundary sliding and diffusional creep, *Metall. Trans.*, **2**(4), 1113–1127, doi:10.1007/BF02664244.
- Ramirez, C., Nyblade, A., Hansen, S. E., Wiens, D. A., Anandakrishnan, S., Aster, R. C., Huerta, A. D., Shore, P., & Wilson, T., 2016. Crustal and upper-mantle structure beneath ice-covered regions in Antarctica from S-wave receiver functions and implications for heat flow, *Geophys. J. Int.*, **204**(3), 1636–1648.

- 727 Randall, G. E., 1994. Efficient calculation of complete differential seismograms for
728 laterally homogeneous earth models, *Geophys. J. Int.*, **118**(1), 245–254.
- 729 Selway, K., 2014. On the Causes of Electrical Conductivity Anomalies in Tectonically
730 Stable Lithosphere, *Surveys in Geophys.*, **35**(1), 219–257, doi:10.1007/s10712-013-
731 9235-1.
- 732 Stevens, N. T., Parizek, B. R., & Alley, R. B., 2016. Enhancement of volcanism and
733 geothermal heat flux by ice-age cycling: A stress modeling study of Greenland, *J.*
734 *Geophys. Res.*, **121**(8), 1456–1471, doi:10.1002/2016JF003855.
- 735 Stixrude, L. & Lithgow-Bertelloni, C., 2005. Mineralogy and elasticity of the
736 oceanic upper mantle: Origin of the low-velocity zone, *J. Geophys. Res.*, **110**(B3),
737 doi:10.1029/2004JB002965.
- 738 Takei, Y. & Holtzman, B. K., 2009. Viscous constitutive relations of solid-liquid
739 composites in terms of grain boundary contiguity: 1. Grain boundary diffusion
740 control model, *J. Geophys. Res.*, **114**(B6), doi:10.1029/2008JB005850.
- 741 Thomas, I. D., King, M. A., Bentley, M. J., Whitehouse, P. L., Penna, N. T.,
742 Williams, S. D. P., Riva, R. E. M., Lavallee, D. A., Clarke, P. J., King, E. C.,
743 Hindmarsh, R. C. A., & Koivula, H., 2011. Widespread low rates of Antarctic
744 glacial isostatic adjustment revealed by GPS observations, *Geophys. Res. Lett.*,
745 **38**(22), doi:10.1029/2011GL049277.
- 746 Thybo, H., 2006. The heterogeneous upper mantle low velocity zone, *Tectonophysics*,
747 **416**(1-4), 53–79, doi:10.1016/j.tecto.2005.11.021.
- 748 Turcotte, D. L. & Schubert, G., 2002. *Geodynamics*, Cambridge University Press,
749 2nd edn.
- 750 van der Wal, W., Whitehouse, P. L., & Schrama, E. J. O., 2015. Effect of GIA
751 models with 3D composite mantle viscosity on GRACE mass balance estimates for
752 Antarctica, *Earth Planet. Sci. Lett.*, **414**, 134–143.

- Wannamaker, P. E., Stodt, J. A., & Olsen, S. L., 1996. Dormant state of rifting
below the Byrd Subglacial Basin, West Antarctica, implied by magnetotelluric
(MT) profiling, *Geophys. Res. Lett.*, **23**(21), 2983–2986, doi:10.1029/96GL02887.
- Whitehouse, P. L., Bentley, M. J., Milne, G. A., King, M. A., & Thomas, I. D.,
2012. A new glacial isostatic adjustment model for Antarctica: calibrated and
tested using observations of relative sea-level change and present-day uplift rates,
Geophys. J. Int., **190**(3), 1464–1482, doi:10.1111/j.1365-246X.2012.05557.x.
- Young, M. K., Tkalčić, H., Rawlinson, N., & Reading, A. M., 2012. Exploiting seismic
signal and noise in an intracratonic environment to constrain crustal structure and
source parameters of infrequent earthquakes, *Geophys. J. Int.*, **188**(3), 1303–1321,
doi:10.1111/j.1365-246X.2011.05326.x.

Figures and Tables

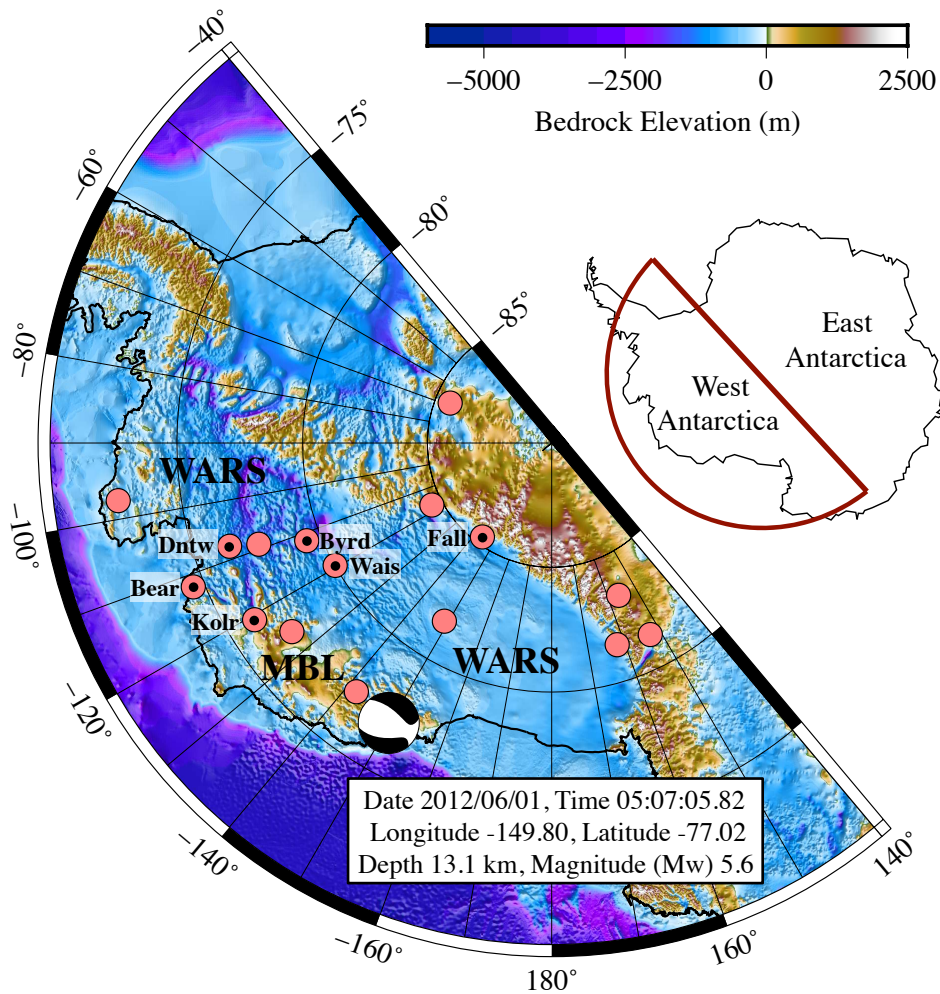


Figure 1: Map showing the locations of POLENET-ANET stations (pink circles) that recorded the 2012 magnitude 5.6 intraplate Marie Byrd Land (MBL) earthquake. The hypocenter and origin time information is from the Global Centroid-Moment-Tensor catalogue. Full waveform modeling of seismograms from the labelled stations were used to infer crustal and upper mantle velocity information for MBL and the West Antarctic Rift System (WARS).

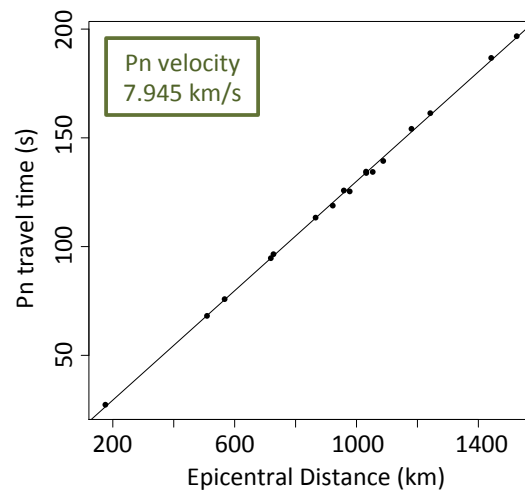


Figure 2: Travel time of the Pn seismic phase from the MBL earthquake to POLENET stations (black circles) as a function of epicentral distance. Linear regression yields an average Pn velocity of ~ 7.95 km/s.

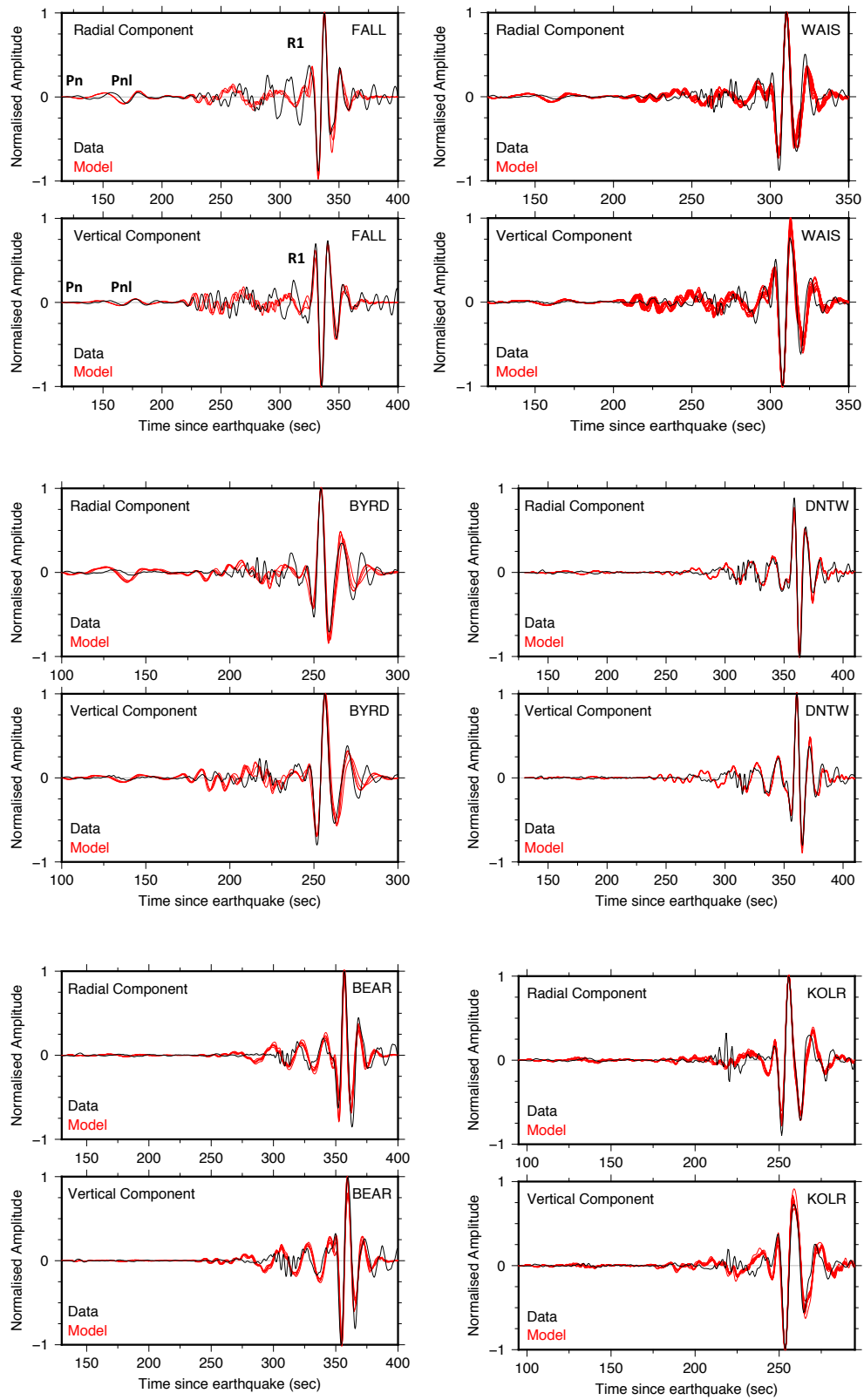


Figure 3: Observed and modeled radial and vertical component seismograms. Station labels are in the upper-right hand corner of each window. The Pn phase, long-period Pnl body-wave and Rayleigh wave (R1) are labelled for station FALL.

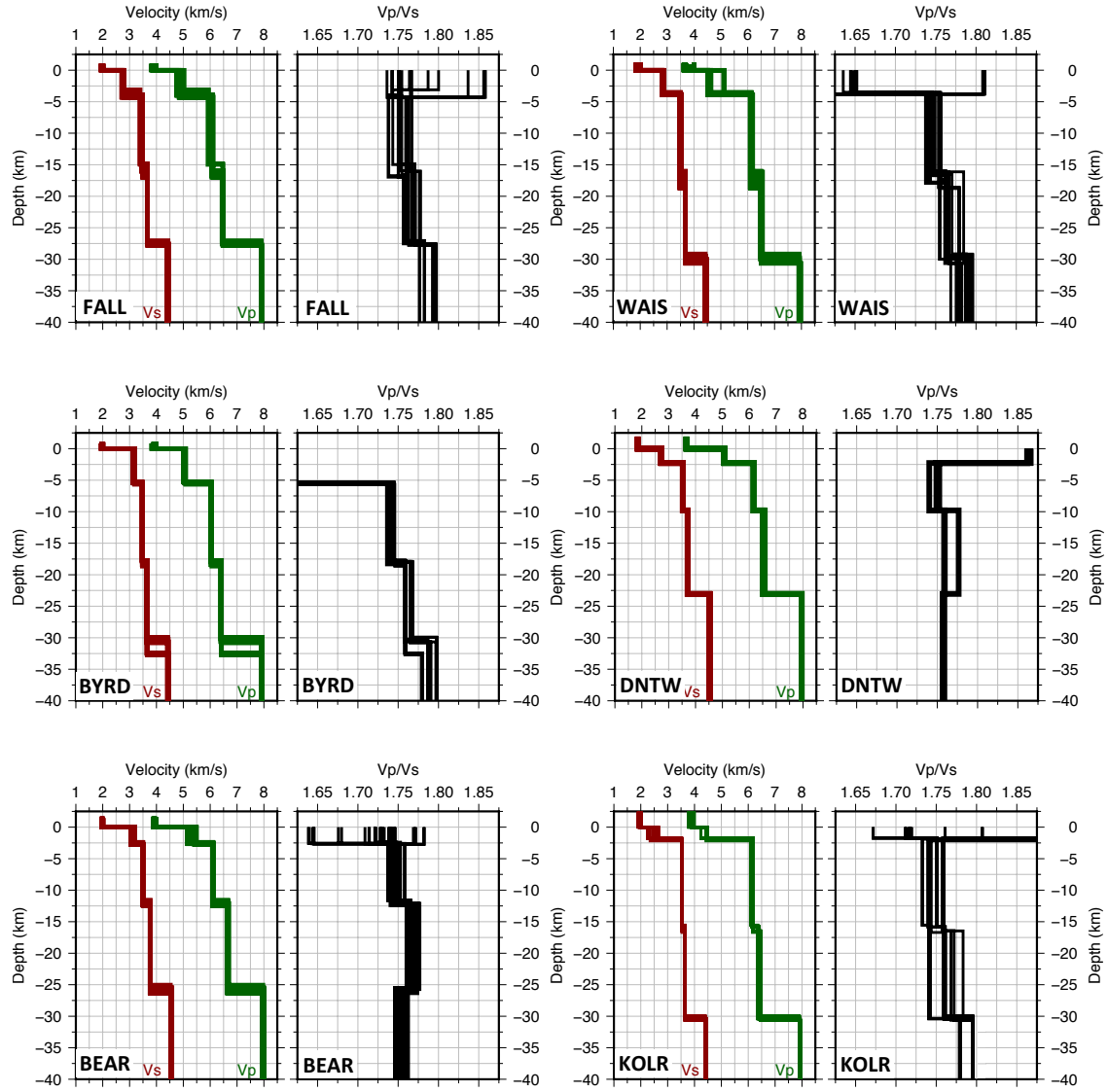


Figure 4: The best generation 1D stratified Earth velocity models (V_P , V_{SV} and V_P/V_{SV}) for each of the earthquake-stations paths. Station labels are in the lower-left hand corner of each window.

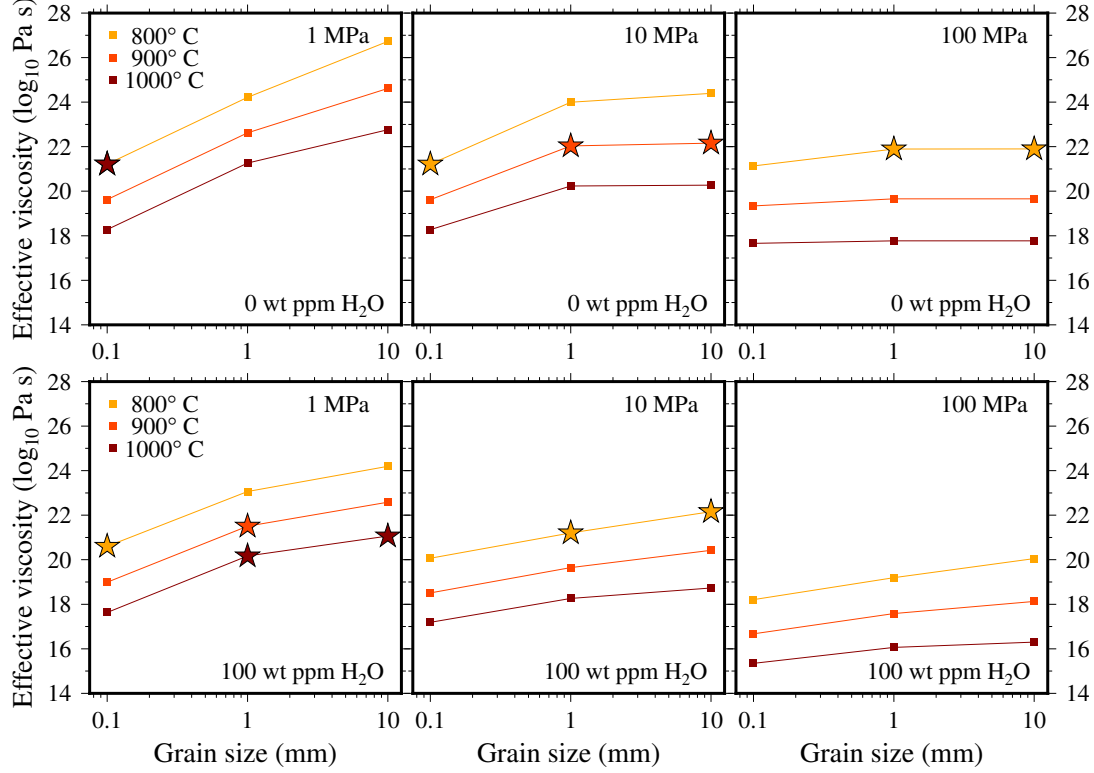


Figure 5: The effective viscosity of the West Antarctic lithospheric mantle as a function of stress, temperature and grain size for both “dry” (0 wt ppm H₂O) and “wet” (100 wt ppm H₂O) conditions. We used Abers & Hacker (2016) to infer a plausible lithospheric mantle temperature range at ~ 50 km depth by matching predicted and observed V_P values for peridotitic rock compositions at a pressure of 1.5 GPa. The inferred V_P range (~ 7.9 - 8.0 km/s) translates to a temperature range of ~ 800 - 1000°C at ~ 50 km depth. Grain size is varied from 0.1-10 mm to encompass grain sizes typically observed in lithospheric mantle xenoliths worldwide. The viscosities were calculated using Equation 2 for representative lithospheric stresses of 1, 10 and 100 MPa at a pressure of 1.5 GPa. Rheological parameters for diffusion creep, dislocation creep and DisGBS regimes taken from Hirth & Kohlstedt (2003), Hansen et al. (2011) and Ohuchi et al. (2015) ($p=3$, $r=0.8$, $n=1$ for diffusion creep; $p=0$, $r=1.2$, $n=3.5$ for dislocation creep; $p=1$, $r=1.25$, $n=3$ for DisGBS). Stars represent solutions giving tectonically plausible strain rates between 10^{-16} and 10^{-14} /s.

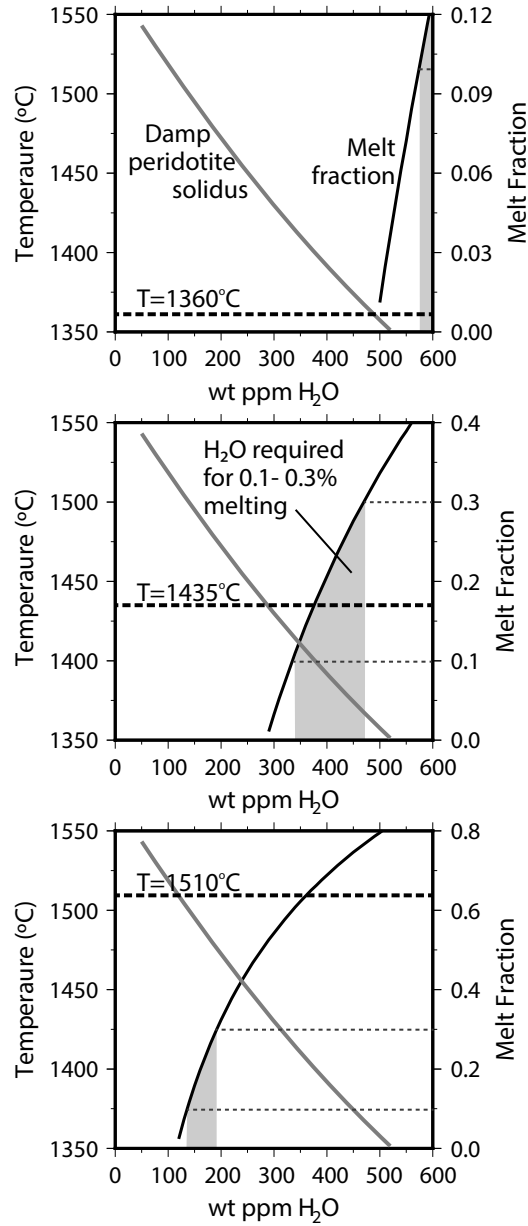


Figure 6: Peridotite solidus and melt fraction as a function of hydrogen content for representative LVZ temperatures of 1360, 1435 and 1515°C at 125 km (~4 GPa). The shaded regions encompass melt fractions of 0.1-0.3%, a range thought consistent with geophysical observations that attribute the origin of the LVZ to the presence of partial melt.

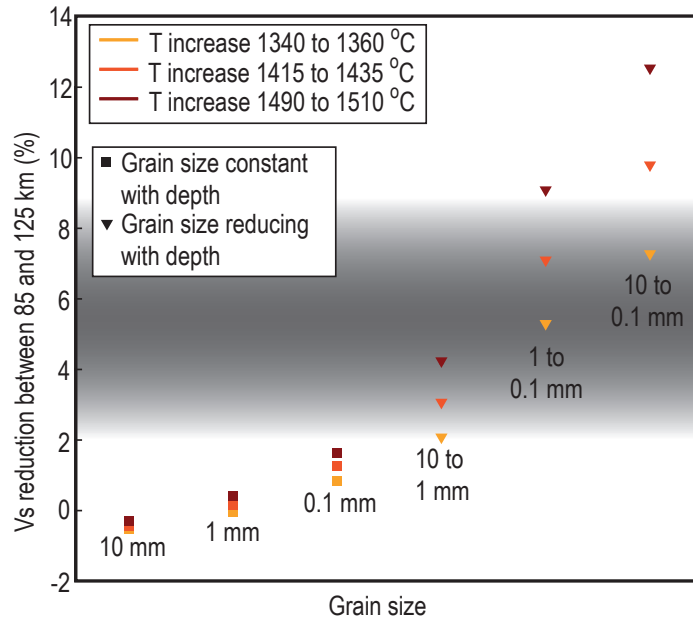


Figure 7: Predicted reduction in shear wave velocity due to the solid-state EAGBS mechanism between 85km depth (at the base of the lithosphere) and 125 km depth (at the centre of the LVZ) for representative temperature and grain size conditions. If grain size does not change from the lithosphere to the LVZ, EAGBS is unlikely to account for the sharp reduction in observed seismic velocities. However, a grain size reduction of one order of magnitude from the lithosphere to the LVZ can easily produce a velocity decrease replicating the observations.

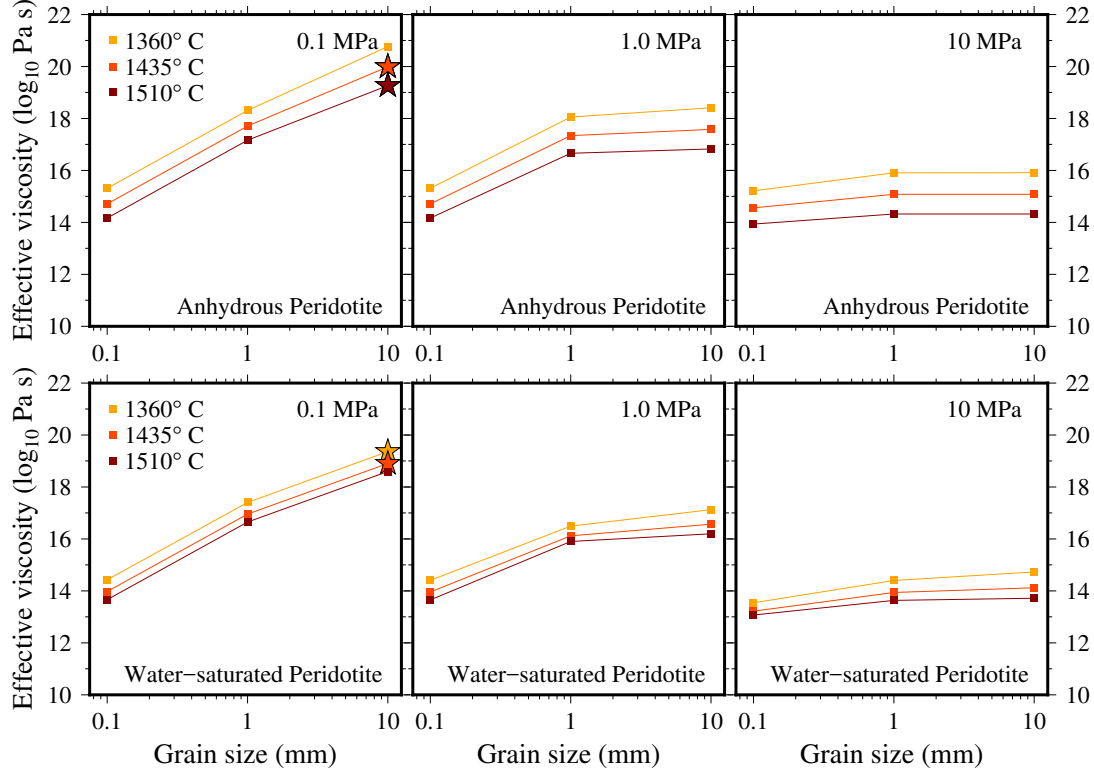


Figure 8: The effective viscosity of the seismic LVZ of West Antarctica as a function of stress, temperature, grain size and hydrogen content for anhydrous and water-saturated peridotite. Taking 85 km as a reasonable average lithospheric thickness for West Antarctica (Heeszel et al., 2016), an assumed mantle potential temperature of ~ 1300 – 1450°C (e.g., O’Reilly & Griffin, 2010) and upper mantle adiabat of 0.4 – $0.5^\circ\text{C}/\text{km}$ (Katsura et al., 2010) translate to a temperature range of ~ 1360 – 1515°C at a depth of 125 km in the center of the LVZ. ~ 490 , 285 and 115 ppm hydrogen are required to lower the peridotite solidus to representative temperatures of 1360, 1435 and 1515°C , respectively. Grain size is varied from 0.1–10 mm. The viscosities were calculated using Equation 2 for representative stresses of 0.1, 1 and 10 MPa at a pressure of 4.0 GPa. Rheological parameters for diffusion creep, dislocation creep and DisGBS regimes taken from Hirth & Kohlstedt (2003), Hansen et al. (2011) and Ohuchi et al. (2015) ($p=3$, $r=0.8$, $n=1$ for diffusion creep; $p=0$, $r=1.2$, $n=3.5$ for dislocation creep; $p=1$, $r=1.25$, $n=3$ for DisGBS). Stars represent solutions giving tectonically plausible strain rates between 10^{-16} and 10^{-14} /s. Viscosities are calculated for a pressure of 4 GPa. The additional effect of partial melt on viscosity is shown in Figure 9.

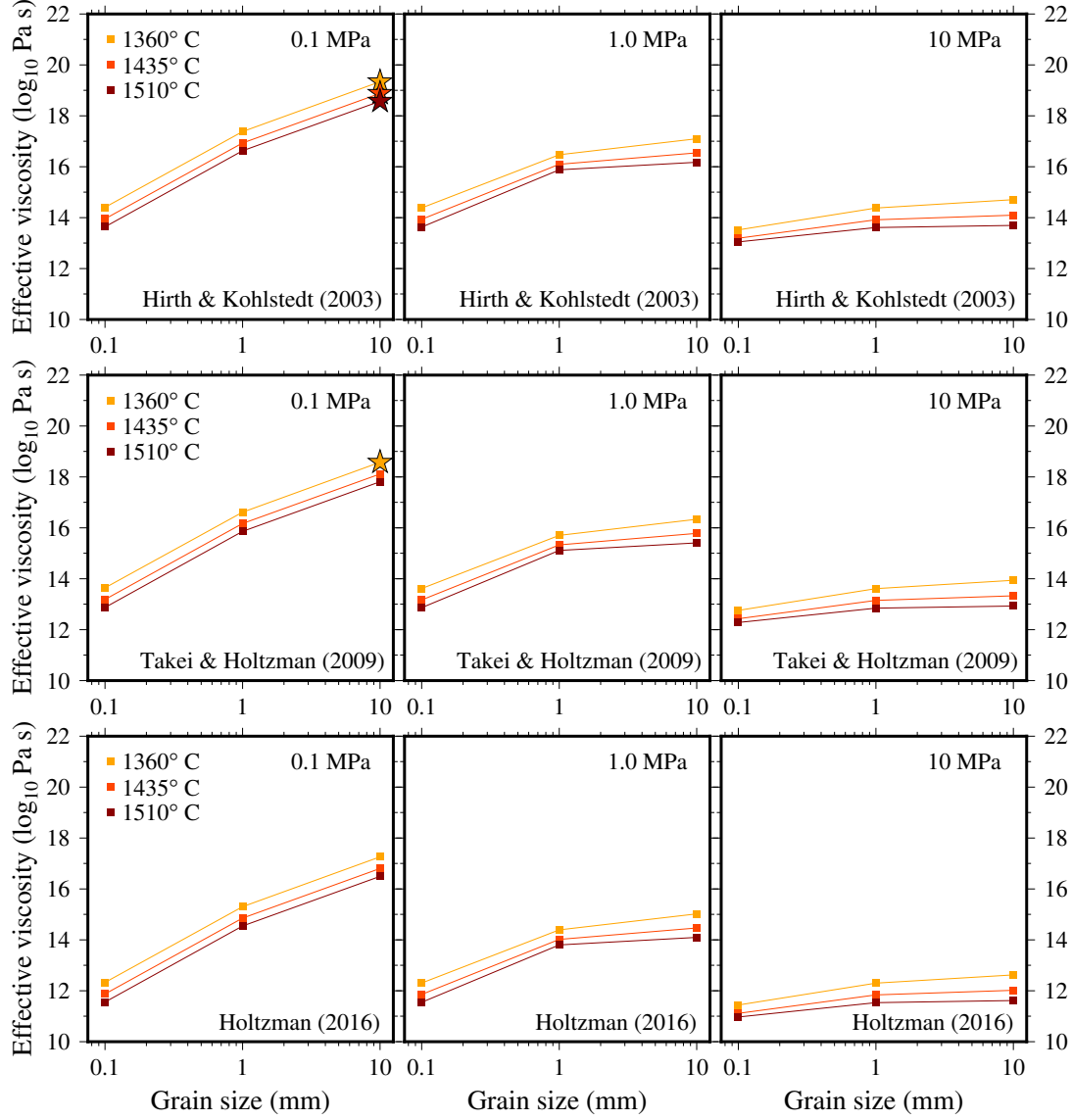


Figure 9: The effective viscosity of the seismic LVZ of West Antarctica as a function of stress, temperature, grain size and hydrogen content for a melt fraction of 0.1%. Solutions are shown for three formulations that quantify the viscosity reduction due to partial melt: Hirth & Kohlstedt (2003), Takei & Holtzman (2009), and Holtzman (2016). Stars represent those solutions giving tectonically plausible strain rates between 10^{-16} and 10^{-14} /s. Viscosities are calculated for a pressure of 4 GPa.

Table 1: Layer thickness (km), V_P (km/s), V_S (km/s) and V_P/V_S ratio constraints that the velocity models had to meet in order to be considered geologically plausible. The constraints are in accordance with the published studies outlined in Section 2.

Earthquake-Station path	FALL	WAIS	BYRD	DNTW	BEAR	KOLR
Ice sheet thickness	0.75 - 1.25	0.75 - 2.50	0.75 - 1.25	1.25 - 2.50	0.75 - 2.25	1.25 - 2.50
Ice sheet V_P	3.5 - 4.0	3.5 - 4.0	3.5 - 4.0	3.5 - 4.0	3.5 - 4.0	3.5 - 4.0
Ice sheet V_P/V_S	1.98	1.98	1.98	1.98	1.98	1.98
Upper crust thickness	1 - 12	1 - 12	1 - 12	1 - 12	1 - 12	1 - 12
Upper crust V_S	2.2 - 3.2	2.2 - 3.2	2.2 - 3.2	2.2 - 3.2	2.2 - 3.2	2.2 - 3.2
Upper crust V_P/V_S	1.55 - 1.90	1.55 - 1.90	1.55 - 1.90	1.55 - 1.90	1.55 - 1.90	1.55 - 1.90
Mid crustal thickness	4 - 20	4 - 20	4 - 20	4 - 20	4 - 20	4 - 20
Mid crustal V_S	3.2 - 3.6	3.2 - 3.6	3.2 - 3.6	3.2 - 3.6	3.2 - 3.6	3.2 - 3.6
Mid crustal V_P/V_S	1.72 - 1.87	1.72 - 1.87	1.72 - 1.87	1.72 - 1.87	1.72 - 1.87	1.72 - 1.87
Lower crustal thickness	4 - 20	4 - 20	4 - 20	4 - 20	4 - 20	4 - 20
Lower crustal V_S	3.6 - 3.8	3.6 - 3.8	3.6 - 3.8	3.6 - 3.8	3.6 - 3.8	3.6 - 3.8
Lower crustal V_P/V_S	1.72 - 1.87	1.72 - 1.87	1.72 - 1.87	1.72 - 1.87	1.72 - 1.87	1.72 - 1.87
Total crustal thickness	22 - 36	22 - 36	22 - 36	22 - 36	22 - 36	22 - 36
Upper mantle V_S	4.4 - 4.8	4.4 - 4.8	4.4 - 4.8	4.4 - 4.8	4.4 - 4.8	4.4 - 4.8
Upper mantle V_P/V_S	1.74 - 1.80	1.74 - 1.80	1.74 - 1.80	1.74 - 1.80	1.74 - 1.80	1.74 - 1.80